K.A. Thomson, K.P. Geigle, M. Köhler, G.J. Smallwood, D.R. Snelling
Optical Properties of Pulse Laser Heated Soot
Appl. Phys. B 104 (2011), 307-319.

The original publication is available at www.springerlink.com

http://dx.doi.org/10.1007/s00340-011-4449-8

Optical Properties of Pulse Laser Heated Soot

K. A. Thomson[1,*], K.P. Geigle[2], M. Köhler[2], G. J. Smallwood[1], D. R. Snelling[1]

[1] National Research Council of Canada (NRC), Ottawa, Canada
[2] German Aerospace Centre (DLR), Stuttgart, Germany

*** Corresponding author:**

Dr. Kevin Thomson
Phone: (613) 991-0868
Fax: (613) 957-7869
Email: Kevin.Thomson@nrc-cnrc.gc.ca

Other authors:

Dr. Klaus Peter Geigle
Phone: ++49/711/6862-398
Fax: ++49/711/6862-578
Email: KlausPeter.Geigle@dlr.de

Dr. Markus Köhler
Phone: ++49/711/6862-756
Fax: ++49/711/6862-578
Email: M.Koehler@dlr.de

Dr. Greg Smallwood
Phone: (613) 993-1391
Fax: (613) 957-7869
Email: Greg.Smallwood@nrc-cnrc.gc.ca

Dr. Dave Snelling
Phone: (613) 993-0810
Fax: (613) 957-7869
Email: Dave.Snelling@nrc-cnrc.gc.ca

PACs: 78.67-Bf, 47.70.Pq, 42.62b

Abstract

To investigate the transient change of soot optical properties resulting from pulsed laser heating of soot in a cooled exhaust plume we have simultaneously performed CW light extinction at 405 and 830 nm and elastic light scattering at 1064 nm. A reversible increase to the 830 nm light extinction of up to 7%, observed during the time period where the soot was hot, suggests a temperature dependent light absorption refractive index function, $E(m_\lambda)$. At low fluence, small permanent increases of $E(m_\lambda)$ of <2% were also observed. 405 nm extinction measurements revealed that the soot likely contained material which continued to absorb 405 nm radiation when desorbed, thus complicating measurement interpretation. 1064 nm light scattering measurements showed a gradual decrease of scattering propensity with increasing laser fluence up to the point of material loss which is consistent with the expected decrease of the structure factor of the soot aggregates as they expand. It is concluded that variations of the optical properties are occurring at the time of LII emission which should be accounted for in time-resolved LII measurement interpretation.

1. Introduction

Soot concentration measurement and particle sizing based on laser-induced incandescence (LII) requires a model which best describes the physical processes involved including the soot properties. A cornerstone of the theory of laser-induced incandescence applied to soot aerosols is that the light

emission properties of soot are not affected by rapid laser heating and thus the measured LII emission can be interpreted to determine the soot temperature, concentration, and active surface area. However, it has been demonstrated in the literature that intense laser irradiances typical of 'high fluence' or 'plateau regime' LII lead to significant modification of the internal structure of soot particles [1] and even the formation of new particles from vaporized material [2]. Even for moderate laser fluences (< 2 mJ/mm^2 @ 1064 nm) typical of auto-compensating LII (AC-LII) [3], subtle morphological changes have been observed via high resolution transmission electron microscopy (HR-TEM) and related changes of emission characteristics for twice heated soot [4]. Permanent and reversible variation of the optical properties of the soot on time scales relevant to LII measurements would change the LII signals and would therefore need to be accounted for in the signal interpretation. Much of the soot modeling in LII is based on graphite properties. Since it is unclear how well graphite describes soot, it is paramount to measure soot properties directly.

In addition to permanent changes to soot structure induced by laser heating as described in [1,2,4], reversible changes in the soot particle light absorption and emission properties related to their expansion and varying temperature must also be considered since the changes would happen on a time scale relevant to the LII emission being measured. The interaction of light with soot aggregates has been demonstrated to be well described by Rayleigh-Debye-Gans Fractal-Aggregate theory (RDG-FA) [5,6]. In this theory, the total light absorption by aggregates is equated to the sum of the light absorption by the individual primary particles. The absorption of the primary particles is described by the Rayleigh limit of Mie theory where light absorption is proportional to the volume of the primary particles interacting with the light.

$$C^{p}_{abs,\lambda} = \frac{\pi^2 d_p{}^3 E(m_\lambda)}{\lambda}, \quad (1)$$

where $C^{p}_{abs,\lambda}$ is the light absorption cross-section, d_p is primary particle diameter, $E(m_\lambda)$, is the soot absorption refractive index function, and λ is the wavelength of light.

While any temporary increase in volume of soot during laser heating will clearly lead to a proportional increase in its volume fraction, an interesting question is whether such a change in the volume of the particle induced by a change in the particle density proportionally changes the light absorbed and emitted by the particle. Alternatively, the volume proportionality in Eq. 1 could be interpreted as a surrogate for the mass of the particle (or the number of atoms or electrons in the particle) and if the mass does not change during an expansion or contraction of the particles, then the light absorption should also remain the same in the absence of a change of the refractive index function $E(m_\lambda)$ with temperature. The precise amount that the volume of soot changes when heated is unclear because of

the complex microstructure of the particles. Michelsen et al. provide various possible thermal expansion coefficient choices which indicate that the volume of soot could change between 6 and 40% when soot is heated from 300 to 4000 K [7]. Since particle expansion could be significant, particle volume change during heating is potentially not an academic point and should be correctly accounted for in the interpretation and modeling of LII emission. It is interesting to note that within the laser-induced incandescence research community, different research groups have, e.g. [8-10], or have not, e.g. [3,11,12], accounted for particle expansion in their description of light absorption and emission from soot particles. In concert with density changes, light absorbed by a particle will also be a function

of its optical properties, specifically $E(m_\lambda)$. If a particle expands due to heating, the distances between

the small scale (i.e., molecular) and the intermediate scale (e.g., planar graphitic microcrystallites) structures in the particle change and it is reasonable to anticipate that the light absorption refractive

index function, $E(m_\lambda)$ will also change.

If the view is taken that soot is comprised of some carbonaceous material in a matrix, it is possible to apply Maxwell-Garnett theory to predict the variation of the optical properties due to a change of the soot density (*i.e.*, an increase of the spacing of the carbonaceous material in the matrix):

$$\left(\frac{m^2-1}{m^2+2}\right)_{eff} = \frac{\rho(T)}{\rho(T_o)}\left(\frac{m^2-1}{m^2+2}\right), \quad (2)$$

where m is the complex refractive index of the light absorbing carbonaceous material and $\rho(T)$ is its density at temperature T [13,14]. Since $E(m_\lambda)$ is proportional to $\left[(m^2-1)/(m^2+2)\right]_{eff}$, as the volume of the particle increases due to expansion, $E(m_\lambda)$ would proportionally decrease and no enhancement of light absorption would be expected, i.e., the product $d_p^3 E(m_\lambda)$ is constant. Thus, Maxwell-Garnett theory says that light absorption by soot aggregates is proportional to the mass rather than the volume of the primary particles.

Amongst the LII community, all groups make the assumption that $E(m_\lambda)$ is invariant with temperature over the broad temperature range experienced by laser heated particles (e.g., [3,7,9,10,12,15-17]). If Maxwell-Garnett theory is indeed correct then the assumption of a constant $E(m_\lambda)$ necessitates the additional assumption of a particle size invariant with temperature to predict light absorption and emission, which scale as $d_\mathrm{p}^3 E(m_\lambda)$. Conversely, if the model employed includes a temperature dependent d_p, it seems necessary that it also includes a density dependent $E(m_\lambda)$.

The description of light scattering by soot aggregates and the influence of particle expansion on that scattering are more complex, however, like light absorption, the scattering intensity of the aggregate scales with the scattering propensity of the primary particles which make up the aggregate.

$$C^{p}_{sca,\lambda} = k^4 \left(d_p/2\right)^6 F(m_\lambda) \tag{3}$$

where $C^{p}_{sca,\lambda}$ is the scattering cross-section of a primary particle, $k = 2\pi/\lambda$ is the magnitude of scattering wave vector of the incident light, and $F(m_\lambda)$ is the soot scattering refractive index function.

It is observed from Eq. 3 that the light scattering scales with the square of the primary particle volume. However, since $F(m_\lambda)$ is proportional to the square of $\left[(m^2-1)/(m^2+2)\right]_{eff}$, Maxwell-Garnett

theory again predicts a compensatory effect where this term exactly cancels the scattering dependence with d_p.

Aggregation is principally accounted for in the scattering cross-section by a structure factor term $S(qR_g)$.

$$C_{sca,\lambda}^{agg} = N^2 S(qR_g) C_{sca,N}^{p} \quad (4)$$

where N is the number of primary particle in the aggregate, the radius of gyration, R_g, is linearly proportional to d_p and $q = (4\pi/\lambda)\sin(\theta/2)$ is the scattering vector for scattering angle θ. As d_p and

R_g increase with particle heating, the structure factor decreases. Thus, when considering both the primary particle scattering coefficient and the structure factor, the aggregate scattering propensity is expected to decrease with particle expansion. Absorption and scattering theory are discussed in greater detail in the theory section.

Several researchers have investigated the influence of laser pulse heating of in-flame soot on light absorption and/or scattering properties. Witze et al. performed simultaneous LII, elastic light scattering (ELS), and laser pulse integrated light extinction measurements of 1064 nm laser heated soot as a function of the laser fluence [18]. Interpretation of the LII measurements in terms of absorption coefficients is difficult since temperature was not measured; however, they show the 90^o scattering coefficient to be invariant with laser fluence for a fluence range of 0.2 – 1.2 mJ/mm^2, in line with the predictions of Maxwell-Garnett theory. Above this fluence, it is likely that material loss due to soot sublimation contributed to the decrease of the scattering coefficient with increasing fluence. The laser attenuation measurements show that the light extinction coefficient increases 20 – 25% over the unheated soot case as the laser fluence is increased to 1 mJ/mm^2. The authors attribute this to particle volume changes and suggest that thermal annealing is a probable cause for the increase. Yoder et al. used a pulsed 1064 nm laser to heat soot and a pulsed 532 nm frequency doubled laser to monitor

elastic light scattering [19]. The timing of the 532 nm laser was adjusted through a range of just before to just after the 1064 nm pulse and it was shown the scattering coefficient is constant throughout the soot heating and early cooling for laser fluences below 1 mJ/mm^2. More recently, Snelling et al. have studied elastic light scatter combined with LII (ES-LII) [20]. They noted that scattering intensity at 35 and 145 degrees increased as a function of laser fluence and found that the laser fluence normalized scattering was constant over a fluence range of 0.1 to 1.6 mJ/mm^2 (532 nm excitation).

Vander Wal and Jensen have also studied the influence of 1064 nm laser heating on soot incandescence [21]. Using two lasers they heated soot twice in rapid succession, comparing the emission induced during the first pulse versus during the second. For the lowest fluence tested (0.9 mJ/mm^2) the intensity recorded at each location in the flame was very consistent between the first and second pulse. For all higher fluences, differences were observed for most flame locations with the incandescence intensity lower during the second pulse, suggesting some change to the optical and/or physical properties of the soot as a consequence of 1064 nm pulsed laser heating with fluences above 0.9 mJ/mm^2. In a related work, Vander Wal et al. used the two laser system to further quantify permanent changes to soot properties induced by laser heating. They observed that for modest heating with the first laser pulse (~1 mJ/mm^2) the signal induced by the second pulse is enhanced, indicating that annealing and graphitization could be leading to enhanced absorption and emission characteristics in the soot [4]. TEM images shown for moderately higher laser fluence indicate that the soot particle perimeter remains unchanged, while the primary particle's internal structure becomes irreversibly modified. Graphitization leads to more pronounced shell structure in the primary particle's perimeter while the core appears hollow. In accordance with [2], fluences beyond approx. 3 mJ/mm^2 lead to increasing mass loss visualized by TEM and decrease of the LII intensity induced by the second,

monitoring laser pulse. However, optical properties or particle temperature during the LII process as required for validation of LII modelling are not explicitly measured and arguments are based only on the LII peak intensity and decay curves.

More recently, Michelsen et al. studied the wavelength and temperature dependence of the absorption and scattering cross sections of soot [7]. Following the methodology developed by Therssen et al. [22], the ratio of $E(m_\lambda)$ at the wavelengths of 532 and 1064 nm was determined by comparing the fluences needed at these two wavelengths to heat the soot such that the same LII emission was observed. Pulse integrated light extinction measurements were then performed at the two wavelengths over a range of fluences. Similar to the results of Witze et al. [18], a ~11% enhancement of the extinction coefficient was initially observed as the 1064 nm laser fluence was increased to ~2 mJ/mm^2, beyond which the extinction coefficient decreased, presumably due to soot sublimation. The data was combined with soot morphology from the literature [23] and RDG-FA theory to determine single scattering albedos, the ratio of $F(m_\lambda)$ to $E(m_\lambda)$, and estimates of the primary particle size change as a function of laser fluence; however, this portion of the analysis relied

heavily on an implicit assumption of a wavelength independent $F(m_\lambda)$ and on soot morphology taken from published results for similar flames. Michelsen et al. determined higher scattering albedo and $F(m_\lambda)$ to $E(m_\lambda)$ ratios than available in the literature. They also found that the particle size variation that they predicted based on light scattering theory was contradictory to that which they predicted based on light absorption [7].

In summary, the literature suggests that for 1064 nm laser fluences below 1 mJ/mm^2, the scattering coefficient of in-flame soot does not vary with fluence despite the expectation that it will drop due to changes in the structure factor. Pulse integrated light extinction measurements suggest a small increase to the extinction coefficient with increasing fluence for the same fluence range. It is not clear from the laser pulse integrated measurements whether the increase of the extinction coefficient is permanent, suggesting a change to the internal structure of the soot, or reversible (i.e. an enhancement only when the soot is heated above the ambient temperature). Therefore, the present work explores further the question of light absorption and scattering by laser heated particles to provide useful experimental data to aid in resolving the above discussion and to determine if variation of optical properties of soot during the LII process must be accounted for in the interpretation of LII

emission signals. Whereas the previous studies have used pulse averaged extinction measurements, in the present study extinction coefficient of a soot aerosol were monitored as a function of time while simultaneously heating the aerosol with laser pulse fluences typical of LII. Continuous measurements (cw) were made of the extinction coefficient at wavelengths of 405 and 830 nm and for a range of (pulsed) laser fluences. Scattering of the 1064 nm heating pulse by the soot was also monitored at 90 degrees to the laser propagation axis. The variation of the extinction and scattering coefficients during and after laser heating was used to explore the interplay of soot particle size variation with heating, elastic and plastic variation of the soot refractive index absorption function, desorption and dissipation of adsorbed species, and sublimation and ultimately to determine whether variation of soot optical properties during the time window of LII emission must be accounted for when interpreting the measurement. While TEM measurements of laser-heated soot as available in literature give a qualitative impression of morphological changes upon varying laser fluence, extinction and scattering measurements allow for better quantification and real-time understanding of optical changes induce by the LII laser pulse.

2. Theory

Visible or near-infrared light attenuation is often used as a diagnostic for soot aerosol measurements since soot is a strong light absorber and a weaker light scatterer [24-28]. Thus, the interpretation of light absorption measurements can be relatively straight forward despite the complex morphology of soot aggregates. Light attenuation is related to the extinction coefficient of the attenuating material, $K_{ext,\lambda}$, via Beer-Lambert theory as:

$$I_\lambda / I_{\lambda,0} = \exp\left(-\int K_{ext,\lambda} dx\right), \quad (5)$$

where $I_{\lambda,0}$ is the intensity of light before transmitting through the medium, I_λ is the light intensity after,

and x is the optical axis. For a homogeneous medium of known length, L,

$$K_{ext,\lambda} = \frac{-\ln\left(I_\lambda / I_{\lambda,0}\right)}{L}, \quad (6)$$

and

$$K_{ext,\lambda} = K_{abs,\lambda} + K_{sca,\lambda} = K_{abs,\lambda}(1 + \rho_{sa,\lambda}), \quad (7)$$

where $K_{abs,\lambda}$, is the absorption coefficient, $K_{sca,\lambda}$, is the scattering coefficient, and $\rho_{sa,\lambda}$ is a ratio of the

scattering and absorption coefficients. For small soot aggregates, this ratio approaches zero and scattering can be neglected in a light extinction measurement. For large primary particle size and for

low measurement wavelengths (in the low visible and ultraviolet wavelengths) $\rho_{sa,\lambda}$ can reach values of 0.3 – 0.4 [26-28], thus enhancing light extinction and making measurements more difficult to interpret. For the present measurements where a Gülder burner has been quenched at a height of 42 mm, we estimate the primary particle size to be approximately 30 nm [29]. The degree of post-flame aggregation is uncertain, but from unpublished two angle scattering measurements (532 nm $35^o/145^o$)[†] applied to the same quenched flame burner used in the present study where a scattering intensity ratio of 6.9 +/- 1.3 was measured and assuming a log normal aggregate size distribution, the geometric mean number of particles per aggregate, $N_{g,}$ is estimated to be approximately 140 for an assumed distribution width σ_g = 2.1, fractal exponent of D_f = 1.7 and fractal pre-factor k_f = 6.2. If we apply this morphology and with $F(m_\lambda)/E(m_\lambda)$ ratios of 1.56 at 830 nm and 0.81 at 405 nm [26,27] and following the method outlined in [28], the ratios of scattering to absorption are 0.11 and 0.17, respectively, indicating that absorption is the dominant contributor to the light extinction. Thus, measurement of the variation of $K_{ext,\lambda}$ during laser heating is a good surrogate for direct measurement

[†] For more details on the experimental setup for the elastic light scattering measurements, see [20]

of the variation of $K_{abs,\lambda}$. By monitoring attenuation, and thus $K_{abs,\lambda}$ throughout a laser heating event,

where the soot is irradiated by a 1064 nm laser pulse, it is possible to see how it varies as a function of soot temperature and laser fluence.

The light scattering coefficient as a function of the scattering vector q for an aerosol of soot aggregates of varying aggregate size is expressed as:

$$K_{soa,\lambda}^{agg}(q) = N_{agg} C_{soa,\lambda}^{p} \int N^2 P(N) S\left(qR_g\left(N, d_p, D_f, k_f\right)\right) dN, \quad (8)$$

where N_{agg} is the number density of soot aggregates, N is the number of primary particles per aggregate, $P(N)$ is the frequency of aggregates of size N, and S is the structure factor which describes the modulation of scattering intensity as a function of the product of the scattering vector, q, and the

radius of gyration of the aggregate, $R_g = d_p\left(N/k_f\right)^{-D_f}$ [13,14]. While the expression is complex, many variables are invariant with soot temperature (i.e. N, N_{agg}, $P(N)$) if the soot aggregates do not fracture during laser heating. Thus, light scattering measurement at 90 degrees will only vary as a function of the primary particle cross-section and the aggregate structure factor. The primary particle scattering cross-section should remain constant with changing primary particle size according to Maxwell-Garnett theory. Conversely, the structure factor is functionally related to R_g which is noted to be linearly proportional to d_p. To understand the influence of particle expansion on the structure

factor it is useful to examine a plot of $S(qR_g)$ versus qR_g, as shown in Figure 1. As particles expand, the product qR_g increases and the structure factor decreases. The sensitivity of S to qR_g depends on the location on the curve, but for the present experimental setup and aggregate size, qR_g varies around 1.5 and for this value there is a near inverse dependence of S to qR_g. . For example, while a 10% increase in d_p results in a 1.7 times increase in d_p^6, the structure factor and thus the overall scattering cross-

section is expected to decrease by 11.2% for 1064 nm scattering at 90 degrees for the above mentioned soot morphology.

In the present measurements, it is not possible to measure the light scattering at the wavelengths of the light attenuation measurements since the cw lasers are not sufficiently powerful to generate a measurable scattering signal relative to the laser induced incandescence signal which occurs during the laser heating. Equally, using a cw laser with sufficient power to allow such a measurement would heat and rapidly oxidize the soot. Instead, we monitor the intensity of 1064 nm light scattered from the pulsed laser used to heat the soot. The measurement is integrated over the duration of the laser pulse and thus represents an average scattering coefficient over a range of soot temperatures. Nonetheless, as the pulse laser fluence is varied, the peak soot temperature achieved varies and knowledge is gained on the influence of soot heating on light scattering.

3. Apparatus

Measurements were performed on cooled soot since the range of temperature variation possible with initially cool soot is greater. The burner used to generate a steady source of cooled soot of long optical path length was a modified Gülder laminar co-annular ethylene/air non-premixed flame burner [30]. Briefly, the burner consists of a central mild steel fuel tube with a 10.9 mm inner diameter surrounded by an annular air nozzle of 88 mm inner diameter[‡]. The air co-flow channel of the burner is fitted with a chimney of 50 mm diameter and 70 mm height which encases the flame. As shown in Fig. 2a, at a

[‡] It is noted that the inner diameter of the air nozzle is incorrectly reported to be 100 mm in [29]

42 mm height above the burner nozzle (HAB) eight 1 mm diameter syringe nozzles point symmetrically toward the vertical axis of the burner in a horizontal plane. Nitrogen jetting from the eight nozzles quenches the flame and creates a steady plume of smoke which then mixes with the co-flowing air. A cap above the burner chimney reduces the diameter of the chimney from 50 mm to 12.5 mm. Above this cap, a T-fitting re-directs the exhaust plume into a horizontal plane (Fig. 2b). The two horizontal exits of the T-fitting include short lengths of 12.5 mm diameter tube. The total length of the horizontal section is 83 mm. The temperature inside the tube was measured to be 533 K. Buoyancy causes the soot to rise above the optical axis after it exits the horizontal section, thus limiting the horizontal path length to ~130 mm with a maximum attenuation of the 1064 nm heating laser of approximately 20% when transmitting through the plume. An extraction hood captures the exhausted gases. The fuel flow rate was 194 ccm (cubic centimeters per minute, 21^{o}C, 1 atm), the air flow rate was 11.5 lpm (liters per minute), and the total nitrogen flow for the quenching jets was 1.5 lpm. In the absence of the quenching jet flow, the visible flame height would have been about 64 mm.

The soot exchange rate in the pipe was estimated through a simple flow calculation involving the exhaust volumetric flow rate, horizontal plume length and cross-sectional area, to be less than 30 milliseconds; sufficiently short to avoid exposure of soot to more than one laser pulse.

The experimental apparatus is shown schematically in Fig. 3. The heating laser was a Big Sky ultra Nd:YAG with a 1064 nm output energy ranging from 2.2 to 31.3 mJ/pulse at 20 Hz with a pulse width of 6.6 ns. The laser energy was controlled by means of a half wave plate and a thin film polarizer. The final polarization direction was selected by a half wave plate and was vertical for all experiments.

A rectangular aperture was inserted in the laser beam. This aperture was imaged at the central vertical axis of the burner using a pair of optically conjugate lenses, generating a beam with a uniform energy distribution in a rectangular profile 2.8 mm wide and 2.8 mm high at the focal point. The beam shape was also relatively constant over the depth-of-field of the horizontal section of the T-fitting as shown in Fig. 4a,e, thus achieving uniform heating of the soot over the intersecting volume of the laser and the horizontal plume. The profiles of the cw lasers are also included in Fig. 4. The cw laser monitored portion of the 1064 nm laser profile is homogeneous to an even higher degree as shown by a histogram of the relative fluence of the pulsed laser for the intersecting region of the pulsed and cw lasers at the fore and back end of the plume (Fig. 4d,h).

Elastic light scattering of the 1064 nm laser heating pulse was monitored at 90 degrees to the laser propagation axis, just upstream of the T-fitting. Scattered radiation was captured by a pair of lens (125 and 150 mm focal length) operated at infinite conjugate and focused onto a 2 mm diameter aperture. A 1064 nm interference filter was placed between the two lenses. A Thorlabs DET-36A biased photo-diode detector (rise time of 14 ns) was placed behind the aperture to monitor the scattered light intensity.

Attenuation measurements through the horizontal plume were achieved at 830 nm and 405 nm using a cw Gallium Arsenide laser and a cw diode laser, respectively. The lasers were transmitted sequentially along the same optical axis as the 1064 nm pulsed laser and the beam profiles were shaped such that the cw laser beams were smaller than the 1064 nm beam. This guaranteed that the cw lasers only monitored the attenuation of the 1064 nm laser heated soot. The transmitted cw laser radiation was monitored by a second Thorlabs DET-36A detector placed 710 mm downstream of the

burner. The detector was fitted with a short focal length lens to focus the cw laser beam onto the detector and an interference filter (sequentially 405 nm and 830 nm for the two attenuation measurement wavelengths). The distance of the detector from the soot plume eliminated laser induced incandescence as a bias from the attenuation measurement as was validated experimentally using the pulsed laser in the absence of the cw laser. The 1064 nm pulse laser radiation was blocked by placing a dichroic beam splitter upstream of the DET-36A detector and a KG-3 filter after the beam splitter.

The signals from the two photodiode detectors were digitized using a LeCroy Waverunner oscilloscope. Data was collected at 200 ns/datapoint and 200 ps/datapoint. Measurements were performed for laser fluences ranging from 0.28 – 4.0 mJ/mm^2 with 400 shot averages acquired for each condition.

4. Results and Discussion

4.1 Light attenuation measurements

An example time-resolved 830 nm transmissivity curve for a laser fluence of 1.4 mJ/mm^2 is included in Fig 5a. A sudden increase of laser transmission is observed at the time of the heating laser pulse, suggesting rapid sublimation of soot or desorption of adsorbed species. It is observed that over a 5 ms time period, the transmissivity returned to the original value, suggesting that all affected soot exits the measurement volume in this time. For the laser pulse frequency of 20 Hz, this indicates that each laser pulse interacts with fresh soot, in agreement with the flow calculations mentioned in the experimental section. If transmissivity is converted to a normalized average extinction coefficient along the measurement chord (normalized to a value of 1 for the period just before the laser pulse), as shown in

Fig. 5b, a rapid decrease 8% of the extinction coefficient is observed which is likely due to soot vaporization.

In Fig. 6, the fast sampling rate normalized extinction coefficient data is shown for the same laser fluence; this corresponds to zooming into the first 1 μs following the laser pulse. It is observed that the variation of extinction coefficient is in fact more complex than was observable in Fig. 5b, with an initial increase over a 50 ns time period before the drop to a similar minimum value as was observed for the low sampling rate data.

Normalized line-averaged 830 nm extinction coefficients are included in Fig. 7. For lower laser fluences, an initial rise of the extinction coefficient over a 30 ns time interval is observed, followed by a gradual decrease towards the initial extinction coefficient over a time period, ~ 1 μs, that corresponds to the cooling time for the laser heated soot. This could result from a small temperature dependence of $E(m_\lambda)$ at 830 nm.

At the highest laser fluences, the initial increase of the extinction coefficient is somewhat suppressed as it is overtaken by a very rapid decrease of the extinction coefficient, likely related to material loss from the soot, followed by a plateau to near constant values over the measurement window shown.

We compare these plateau values to the amount of soot sublimated predicted by LII theory [31] in Fig. 8. The 830 nm extinction measurements have been converted to absorption using Eq. 6 with $\rho_{sa,830\,nm} = 0.11$. The calculations of [29] were done for 532 nm excitation with an E(m) value of 0.4 and a flame temperature of 1730 K . To scale the 532 nm fluence used in the LII model to the 1064 fluence used in the present work we have assumed a wavelength independent $E(m_\lambda)$ and scaled the LII model fluences by a factor of 2 to account for the λ^{-1} dependence of the soot absorption. The fluence

needed to raise the soot temperature from 533 to 1730 K was also considered in the calculation. For $E(m_\lambda)$ = 0.4 the predicted soot evaporation by LII theory is ~ 30% less than predicted by our results if we interpret the plateau values as a result of soot evaporation. By assuming an $E(m_\lambda)$ of 0.55 we get much better agreement between model predictions and our present observations, including the fluence at which material loss is first expected. However, such an $E(m_\lambda)$ is higher than expected from the literature (see [32] and references therein).

Overall, the present 830 nm extinction coefficient measurements are qualitatively consistent with those of Witze et al. and Michelsen et al. [7,18] for 532 nm and 1064 nm. For fluences below 1 mJ/mm^2, an enhancement of the extinction coefficient is observed and above this value, the extinction coefficient falls dramatically. With the current time resolved measurements it can be observed that the majority of the enhancement is reversible in that after several 100 nanoseconds, the extinction coefficient returns to near its original value (Fig. 7a). If a constant $E(m_\lambda)$ is assumed, in disagreement with the predictions of Maxwell-Garnett theory, the enhancement of the extinction coefficient could be plausibly related to the anticipated increase of the particle size during heating. The elastic nature of the enhanced extinction also fits nicely with the particle expansion argument. However, it might equally be argued that Maxwell-Garnett theory is correct and that $E(m_\lambda)$ has a temperature dependence and this is what is detected in the measurements.

Figure 9 includes relative extinction coefficients for the lowest laser fluences for the first 8 μs after the laser pulse. It is noted that the normalized extinction coefficients for 0.55 and 0.83 mJ/mm^2 do not return to a value of 1 in the first 2000 ns, which is sufficient time for the soot to return to the ambient temperature. This suggests the possibility of a small permanent change to the soot, most likely in the

form of an increase to the refractive index function, $E(m_\lambda)$, due to restructuring of the crystalline material in the soot during laser heating. This would be consistent with Vander Wal et al. [4] where it was observed that soot emission was enhanced during a second laser pulse after a low fluences pulse first heated the soot. Between 2000 and 4000 ns, the extinction coefficient drops subtly for all curves. The reason for this drop is not understood at this time. Overall, the increase is 2% or less and will therefore have little impact on LII measurement interpretation. For higher fluences, it is possible that there is additional internal restructuring, but this is not detectable through the extinction measurements since mass loss dominates.

Figure 10 includes normalized average 405 nm extinction coefficients over three time windows for a laser fluence of 1.4 mJ/mm^2. In Fig. 10a, a significant decrease of extinction coefficient is followed by a gradual return to a value of unity as the soot is flushed out of the measurement volume. In comparison to the 830 nm data in Fig. 7, the decrease in extinction coefficient is similar in magnitude, but the time to reach this value is significantly longer (hundreds of microseconds versus hundreds of nanoseconds). In the two zoom plots (Fig. 10b, c) it becomes evident that the extinction coefficient first quickly decreases over a 30 ns time period, then rises within 100-200 ns to a value greater than the initial value and afterwards decreases again over several hundred microseconds observable in Fig. 10a. The feature before the laser pulse as visible in Fig. 10c can be attributed to Q-switch noise.

As discussed for the Fig. 6 visualizing of 830 nm attenuation, sublimation is expected to be present after several 10 nanoseconds. In addition, condensed species adsorbed on the soot surface will be desorbed even at low fluence. If a coating of adsorbed species is preferentially desorbed at lower laser fluences, any enhancement in the extinction coefficient at 405 nm attributable to an increase in the

particle temperature could be overshadowed by the decrease caused by the transformation of 405 nm light absorbing material.

Thus, a possible explanation for the fall then rise in the extinction coefficient observable in Fig. 10b and c, and completely opposite to the behaviour at 830 nm, is that these species leaving the soot surface are less effective absorbers in the gas phase (thus the initial drop of the extinction coefficient); however, these released species interact or relax chemically to form others with a higher propensity to absorb radiation at 405 nm. A recent TOF-MS study of pulse laser heated soot, for example, detected species interpreted as graphene layers in addition to C_n species, $3<n<17$, in the gas phase when soot was irradiated at 1064 nm by very low fluence pulses [33]. Among those, C_3 has a strong absorption peak at 404.977 nm [34] and graphene would also interact strongly with 405 nm radiation. The formation of secondary species would take some time and thus the time delay between the material loss and extinction enhancement. Conversion of amorphous into crystalline sub-units (termed mode A and mode B in [33], and distinguished by physical properties), being one potential realization of "annealing" is another effect expected for high temperatures, having a different time constant than the chemical effects mentioned above and influencing absorptive properties as detailed in [33] and relevant for different profiles monitoring at 830 and 405 nm, respectively. Once the material is completely transformed, or once the soot temperature drops sufficiently, the extinction coefficient stops rising and begins to drop as the gas phase material cools and/or condenses. For the characteristic decay time of about 100 μs, and for typical gases at a temperature of 533 K, it is noted that the mass diffusion length is about 150 μm which is too short to explain a significant diffusive loss of desorbed species from the laser heated volume. Another possible loss mechanism for reactive C_n species is oxidation to form CO and CO_2 [35] which would no longer absorb at 405 nm.

The normalized line-averaged 405 nm extinction coefficients for all fluences and for the long time interval are included in Fig. 11. The curve shapes are generally consistent with the 1.4 mJ/mm^2 case highlighted in Fig. 10a. When compared to the 830 nm data presented in Fig. 7, it is noted that the minimum extinction coefficients achieved at higher laser fluences are not as low for the 405 nm experiment. The variation of the minimum relative extinction coefficients for the two wavelengths is summarized in Fig. 12. It is observed that for fluences up to 1.7 mJ/mm^2, the minimum is fairly consistent for the two wavelengths. Above this fluence, the minimum becomes increasingly lower for the 830 nm data. Again, using the hypothesis that the soot has a surface coating, the shift in trend at 1.7 mJ/mm^2 is possibly explained as a transition from desorption of a surface coating which produces a gas phase species which can be oxidized in a 100-300 μs timescale to sublimation of the core soot material which forms a gas phase species which is not as easily oxidized. Complete oxidation of this other material does not occur or is masked by the replenishment of soot in the measurement volume. Conversely, the exact nature of the desorbed or sublimed material is not a factor for the 830 nm data since the species do not appear to attenuate light at this wavelength and so the drop of the extinction coefficient after laser heating is very fast relative to the soot exchange rate in the tube.

The normalized line-averaged 405 nm extinction coefficients for all fluences and for the short time interval are included in Fig. 13. It is again noted that at the time of the laser pulse, there is a repeatable oscillation to the inferred extinction coefficient which is believed to relate to Q-switch noise interference in the cw laser measurement and should be ignored. Beyond this, it is evident the curves are dramatically different than for 830 nm. For low fluences, there is an initial small decrease of

extinction coefficient peak in the first 30 ns after the laser pulse which is opposite to the increase in the extinction coefficient at 830 nm. For high fluences, there is also an initial rapid drop of the extinction coefficients but not to the same extent as for the 830 measurements (13% drop for 405 nm at 4.0 mJ/mm^2 versus 64% for 830 nm). After the initial drop the 405 nm extinction coefficient rises over a 200 ns time period for both low and high fluence measurements which is not observed at 830 nm. Finally, the extinction coefficient drops to similar minimums for the high fluence measurements, but over a time period 3 orders of magnitude longer than for the 830 nm measurements (Fig. 10a).

The 830 nm extinction data shows a rapid small (≤ 7%) increase of the extinction coefficient at all laser fluences, which might be related to an increase in $E(m_\lambda)$ or alternatively with an increase in primary particle soot diameter with temperature as the soot is heated from ambient to near soot evaporation temperatures. At higher fluence soot sublimation occurs that is consistent with LII modeled soot sublimation, but with an $E(m_\lambda)$ value of 0.55 at 1064 nm. The situation is much less clear at 405 nm where the expected decrease in extinction with soot sublimation is partly masked by an absorption that may be due to species desorbed from the soot particles

4.2 Light scattering measurements

Figure 14 includes a plot of fluence-normalized scattering versus fluence. Besides a rise from the first to the second data point which we attribute to inaccurate determination of the laser fluence at the sensitivity limit of the laser power meter, the scattering propensity of the soot aggregates, i.e. $K_{sca,\lambda}$, tends to decrease with increasing fluence. For fluences below 1.5 mJ/mm^2, the drop is gradual; a 10% drop in the scattering propensity over the fluence range of 0.5 to 1.5 mJ/mm^2. This drop is consistent with the expected result of Maxwell Garnett theory that there should be no enhancement in the

scatter cross-section of the primary particles introduced by their expansion and with RDG-FA theory that the increase in the radius of gyration of the aggregates will have an inverse influence on the structure factor and consequently lead to a drop in the scattering propensity of the aggregates. For fluences above 1.5 mJ/mm^2 the more rapid reduction of scattering propensity is attributed to material loss. This is consistent with the 830 nm extinction measurements where mass loss was detected for fluences as low as 1.1 mJ/mm^2. The present observed trend of decreasing scattering propensity with increased heating for low laser fluences is inconsistent with the previous measurements of Witze et al., Yoder et al., and Snelling et al. [18-20] where no decrease of scattering propensity with fluence was observed for fluences below 1.0 mJ/mm^2. The reasons for this difference are not understood at this time; however, it is noted the present measurements were performed for cold soot for which changes in particle size before sublimation would be more dramatic.

5. Conclusions and Perspective

In this work, we examined light interaction with soot particles during a rapid laser heating event. We aimed to understand if light absorption and scattering scale with the volume and square of the volume of the soot particles, respectively or if it is more closely related to the optical properties of soot. We also hoped to detect any permanent changes in soot optical properties brought on by the rapid change of temperature. Unfortunately, the measurements are not sufficient to entirely resolve these questions, but they do offer several important insights:

1.) Based on 830 nm extinction measurements, enhanced light absorption is observed during soot heating and the magnitude could be explained by thermal expansion of soot particles but could equally be related to a temperature dependent $E(m_\lambda)$

2.) Absorption coefficient variation should be accounted for in LII models in the laser light absorption term and the incandescent emission term

3.) A permanent increase of $E(m_\lambda)$ of 2% or less, likely related to soot graphitization, is observed

4.) Based on 830 nm extinction, the onset of material loss occurs at a fluence as low as 1.0 mJ/mm^2

5.) 405 nm extinction measurements suggests that desorbed and vaporized transient species partly absorb 405 nm radiation in the gas-phase

6.) 1064 nm light scattering efficiency does not increase with particle size increase and is therefore more likely proportional to the amount of material in the particle (i.e mass) rather than the volume (for particles in the Rayleigh limit) in agreement with Maxwell-Garnet theory.

7.) Scattering does decrease slowly with increasing laser fluence which is consistent with the prediction of RDG-FA theory and the structure factor

In conclusion, the optical properties of soot change on a time scale relevant to LII emission measurement and must be correctly accounted for in LII emission models. Future measurements will include a more detailed study of the scattering fluence dependence for low fluences, attenuation measurements at other wavelengths, and the study of in-flame soot to see if the presence of adsorbed species on soot is principally a consequence of the flame quenching and subsequent cooling in the flow tube.

Acknowledgements

The authors acknowledge the support of a Helmholtz/NRC collaborative partnership which made this research possible. We also thank Daniel Gareau for his contributions to the experimental setup, Oleksiy Kochevskyy for detailed flow calculations not shown here and Dr. Christopher Sorensen for many helpful discussions on light scattering, particularly on the application of Maxwell Garnett theory to soot optical properties.

References

[1] R. L. Vander Wal, Carbon **37**, 231-239 (1999).

[2] H. A. Michelsen, A. V. Tivanski, M. K. Gilles, L. H. van Poppel, M. A. Dansson, and P. R. Buseck, Appl Optics **46**, 959-977 (2007).

[3] D. R. Snelling, G. J. Smallwood, F. Liu, O. L. Gülder, and W. D. Bachalo, Appl Optics **44**, 6773-6785 (2005).

[4] R. Vander Wal, T. Ticich, A. Stephens, Appl Physics B-Laser O **67**, 115-123 (1998)

[5] F. Liu and D. R. Snelling, in *40th Thermophysics Conference, American Institute For Aeronautics and Astronautics, 2008-4362* (2008).

[6] T.L. Farias, Ü.Ö. Köylü, and M.G. Carvalho, Appl Optics **35**, 6560-6567 (1996).

[7] H. A. Michelsen, P. E. Schrader, and F. Goulay, Carbon **48**, 2175-2191 (2010).

[8] H. A. Michelsen, J Chem Phys **118**, 7012-7045 (2003).

[9] H. Bladh, P.-E. Bengtsson, J. Delhay, Y. Bouvier, E. Therssen, and P. Desgroux, Appl Phys B-Lasers O **83**, 423-433 (2006).

[10] R. Hadef, K.-P. Geigle, W. Meier, and M. Aigner, Int J Therm Sci **49**, 1457-1467 (2010).

[11] H. Bladh and P.-E. Bengtsson, Appl Phys B-Lasers O **78**, 241-248 (2004).

[12] M. Hofmann, B.F. Kock, T. Dreier, H. Jander, and C. Schulz, Appl Phys B-Lasers O **90**, 629-639 (2008).

[13] C. F. Bohren and D. R. Huffman, *Absorption and Scattering of Light By Small Particles* (John Wiley & Sons, Inc., New York, 1983).

[14] C. M. Sorensen, Aerosol Sci Tech **35**, 648-687 (2001).

[15] J. Reimann, S.-A. Kuhlmann, and S. Will, Appl Phys B-Lasers O **96**, 583-592 (2009).

[16] H. Bockhorn, H. Geitlinger, B. Jungfleisch, Th. Lehre, A. Schön, Th. Streibel, and R. Suntz, Phys Chem Chem Phys **4**, 3780-3793 (2002).

[17] R. L. Vander Wal and T. M. Ticich, Appl Optics **38**, 1444-1451 (1999).

[18] P. O. Witze, S. Hochgreb, D. Kayes, H. A. Michelsen, and C. R. Shaddix, Appl Optics **40**, 2443-2452 (2001).

[19] G. D. Yoder, P. K. Diwakar, and D. W. Hahn, Appl Optics **44**, 4211-4219 (2005).

[20] D. R. Snelling, O. Link, K. A. Thomson, and G. J. Smallwood, *submitted* Appl Phys B-Lasers O, October 2010.

[21] R. L. Vander Wal and K. A. Jensen, Appl Optics **37**, 1607-1616 (1998).

[22] E. Therssen, Y. Bouvier, C. Schoemaecker-Moreau, X. Mercier, P. Desgroux, M. Ziskind, and C. Focsa, Appl Phys B-Lasers O **89**, 417-427 (2007).

[23] R. Puri, T. F. Richardson, and R. J. Santoro, Combust Flame **92**, 320-333 (1993).

[24] Ü. Ö. Köylü, Combust Flame **109**, 488-500 (1996).

[25] J. Zerbs, K. P. Geigle, O. Lammel, J. Hader, R. Stirn, R. Hadef, W. Meier, Appl Phys B-Lasers O **96,** 683-694 (2009)

[26] S. S. Krishnan, K.-C. Lin, and G. M. Faeth, J Heat Transf **122**, 517-524 (2000).

[27] S. S. Krishnan, K Lin, and G M Faeth, J Heat Transf **123**, 331-339 (2001).

[28] A. R. Coderre, K. A. Thomson, D. R. Snelling, M. R. Johnson, Spectrally-Resolved Light Absorption Properties of Cooled Soot From a Methane Flame, submitted Appl Phys B, October 2010

[29] K. Tian, F. Liu, K. Thomson, D. Snelling, G. Smallwood, and D. Wang, Combust Flame **138**, 195-198 (2004).

[30] D.R. Snelling, K. A. Thomson, G. J. Smallwood, Ö. L. Gülder, Appl Optics **38**, 2478-2485 (1999)

[31] D. R. Snelling, K. A. Thomson, F. Liu, and G. J. Smallwood, Appl Phys B-Lasers O **96**, 657-669 (2009).

[32] B. M. Crosland, M. R. Johnson, and K. A. Thomson, *accepted* Appl Phys B-Lasers O, DOI 10.1007/s00340-010-4130-7

[33] H. -H. Grotheer, K. Wolf, and K. Hoffmann, Photoionization Mass Spectrometry for the Investigation of Combustion Generated Nascent Nanoparticles and their Relation to Laser Induced Incandescence, *submitted* Appl Phys B-Lasers O, September 2010.

[34] A. E. Douglas, Astrophys J **114**, 467-470 (1951).

[35] R. T. Meyer, A. W. Lynch, and J. M. Freese, J Chem Phys **77**, 1083-1092 (1973).

List of Figures

Figure 5 – samples of time resolved (a) 830 nm transmissivity and (b) average extinction coefficient for a 1.4 mJ/mm^2 laser pulse

Figure 6 – example of time resolved line-averaged 830 nm extinction coefficient for a 1.4 mJ/mm^2 laser pulse

Figure 7 – normalized line-averaged 830 nm extinction coefficients for a range of pulse laser fluences

Figure 8 – soot material loss estimated from plateau in 830 nm extinction measurements (for $\rho_{sa,830nm}$ = 0.11) and from LII simulation with $E(m_\lambda)$ = 0.4 and 0.55

Figure 9 – normalized line-averaged 830 nm extinction coefficients for a range of pulse laser fluences

Figure 10 – normalized line-averaged 405 nm extinction coefficients for a laser fluence of 1.4 mJ/mm^2 for (a) long, (b) mid, and (c) short time intervals

Figure 11 - normalized line-averaged 405 nm extinction coefficients for a range of pulse laser fluences (long time interval)

Figure 12 – minimum of normalized line-averaged 405 nm (300 μs after laser pulse) and 830 nm (1 μs after laser pulse) extinction coefficients for a range of pulse laser fluences

Figure 13 – normalized line-averaged 405 nm extinction coefficients for a range of pulse laser fluences (short time interval)

Figure 14 – normalized 1064 nm scattering intensity (measured scattering/fluence) versus fluence

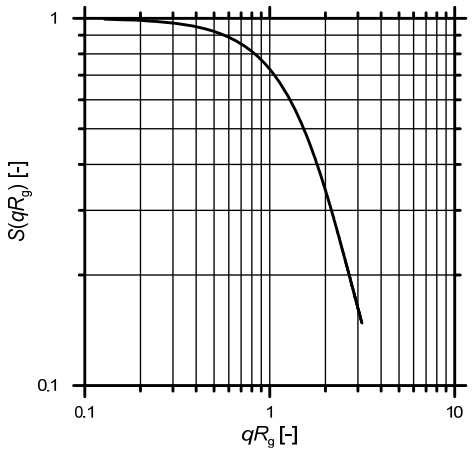

Figure 1 – Structure factor for soot aggregates as a function of qR_g.

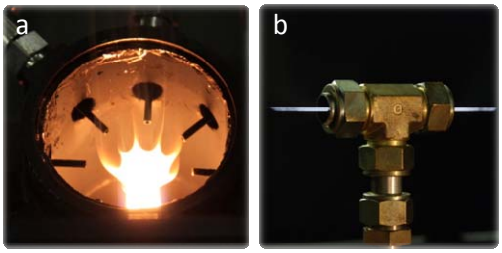

Figure 2 – (a) burner chimney with 8 nozzles and (b) converging 'cap' attached above the nozzle (not shown) and T-fitting create a horizontal plume of soot. Incandescent emission of the laser heated soot in the plume is visible in the photograph as a horizontal line.

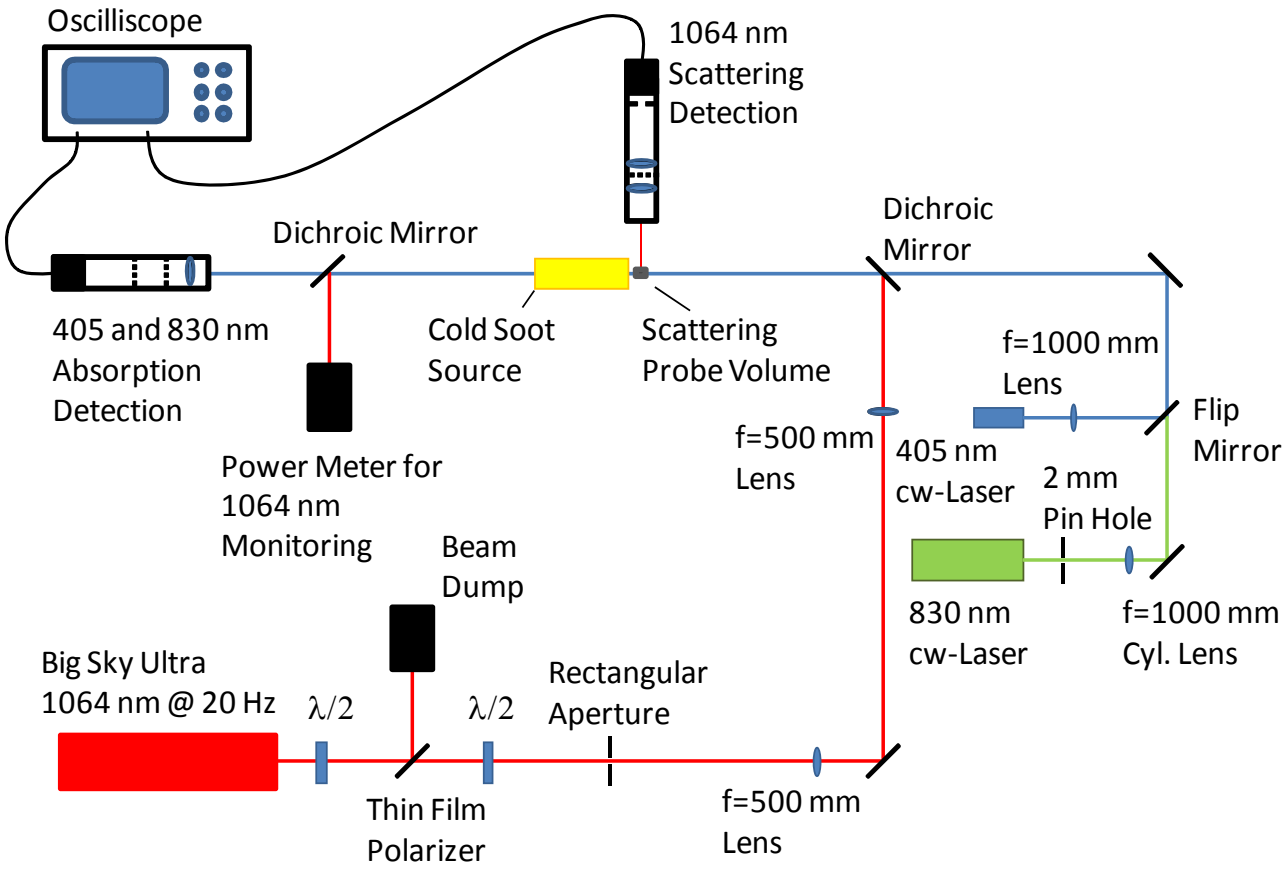

Figure 3 – experimental layout

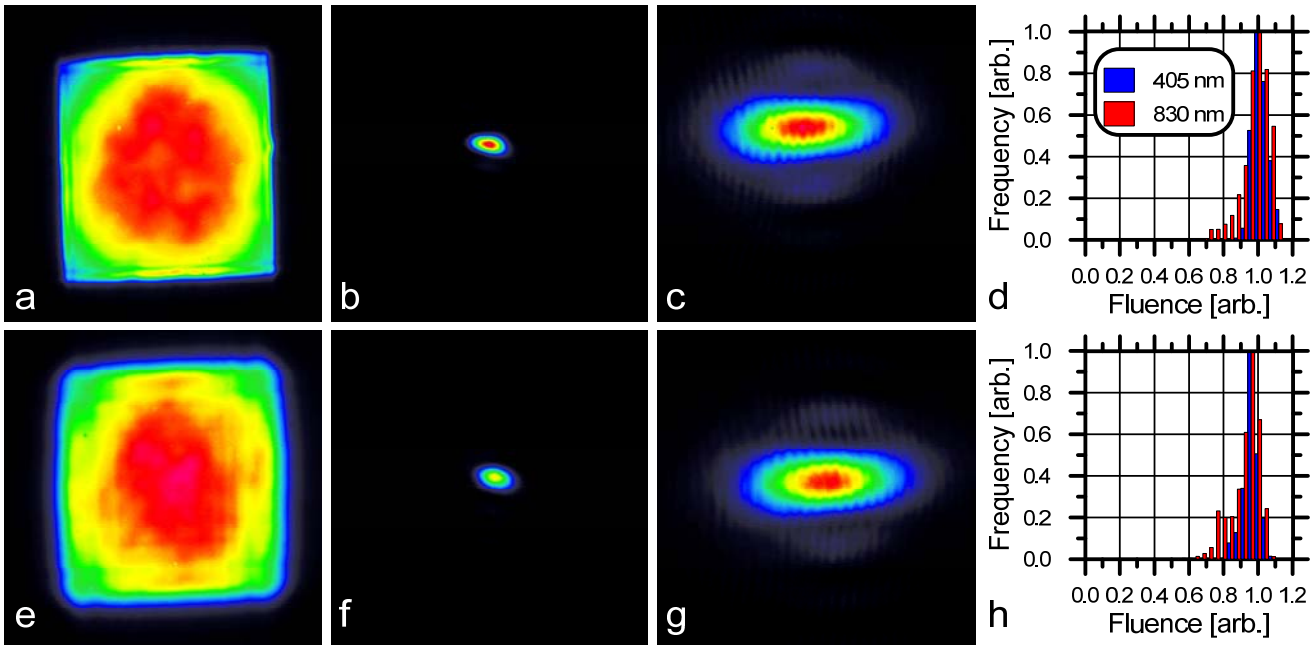

Figure 4 – beam profiles of 1064 nm pulse laser, 405 cw laser, and 830 cw laser (a, b, c, respectively) and histogram of the relative 1064 nm laser fluence in the intersecting region of the pulsed and cw lasers (d) at the fore end of the horizontal plume and the same for the back end of the plume (e, f, g, h, respectively)

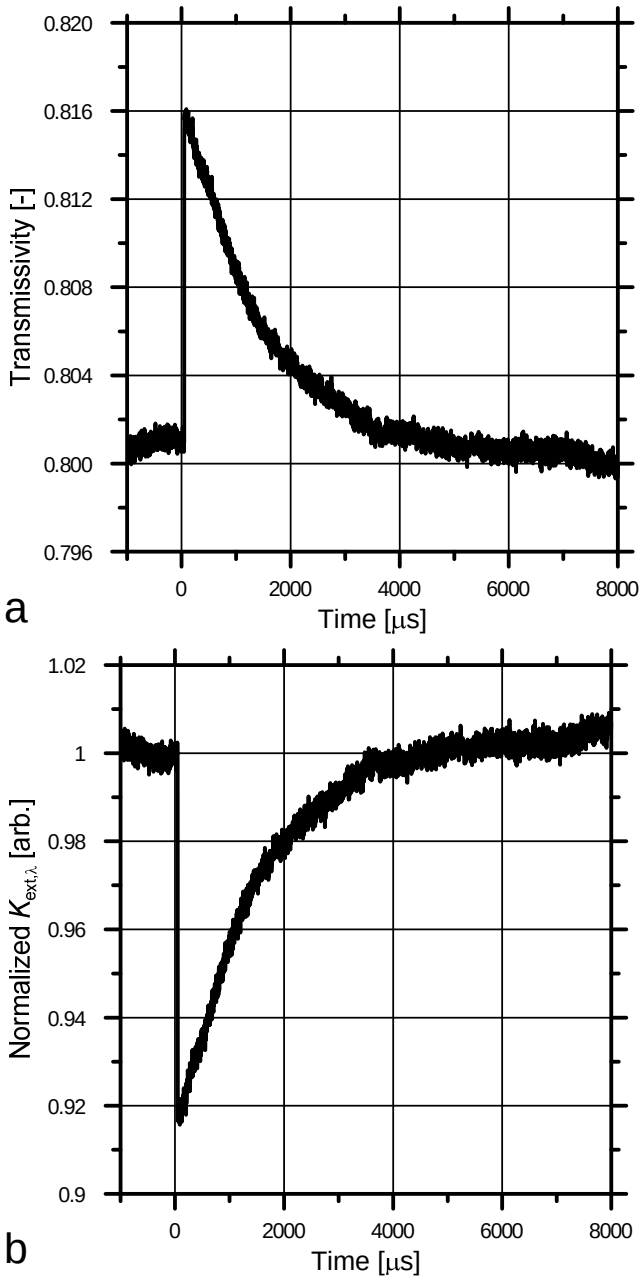

Figure 5 – samples of time resolved (a) 830 nm transmissivity and (b) average extinction coefficient for a 1.4 mJ/mm² laser pulse

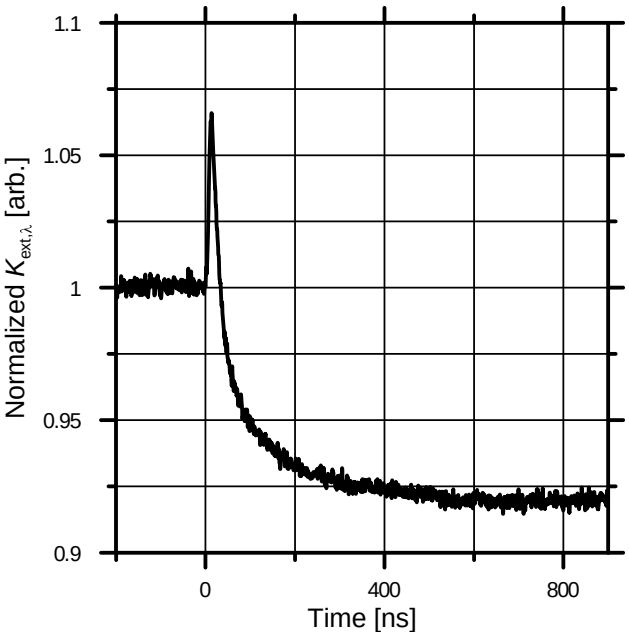

Figure 6 – example of time resolved line-averaged 830 nm extinction coefficient for a 1.4 mJ/mm² laser pulse

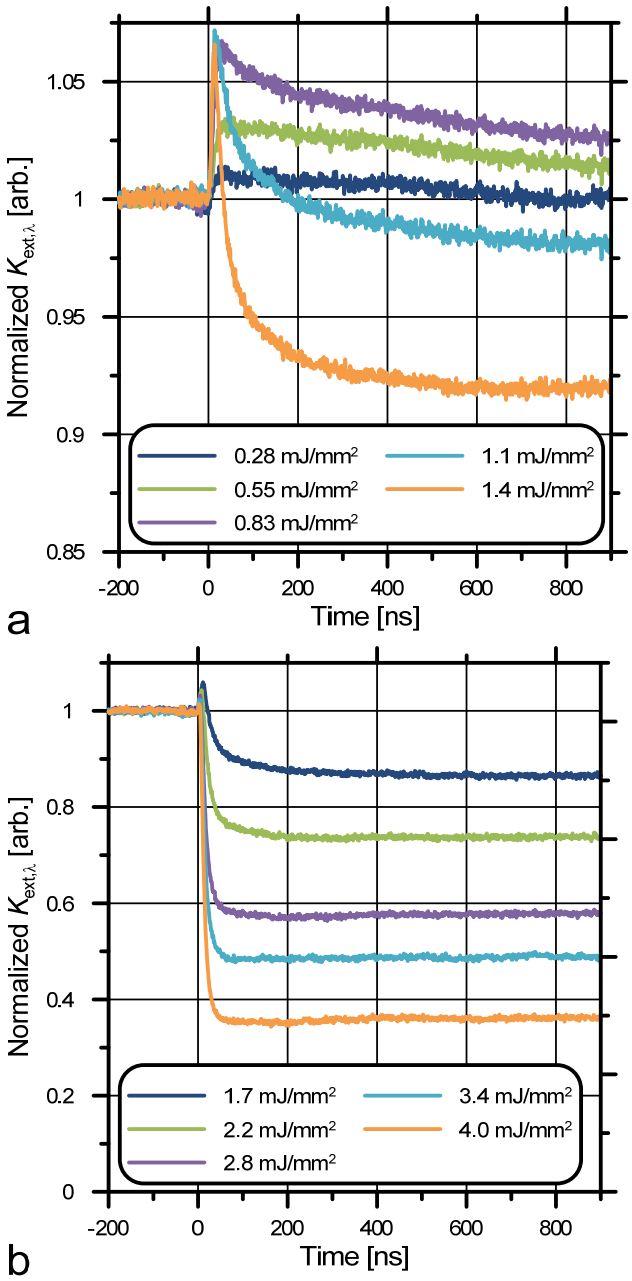

Figure 7 – normalized line-averaged 830 nm extinction coefficients for a range of pulse laser fluences

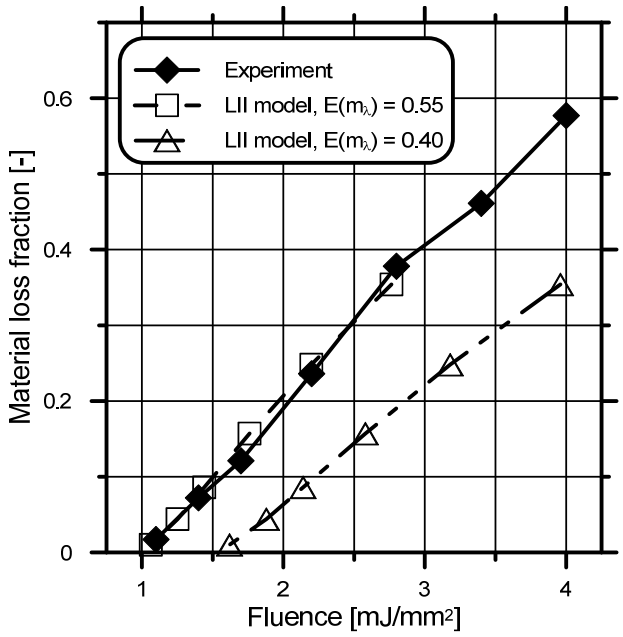

Figure 8 – soot material loss estimated from plateau in 830 nm extinction measurements (for $\rho_{sa,830nm}$ = 0.11) and from LII simulation with $E(m_\lambda)$ = 0.4 and 0.55

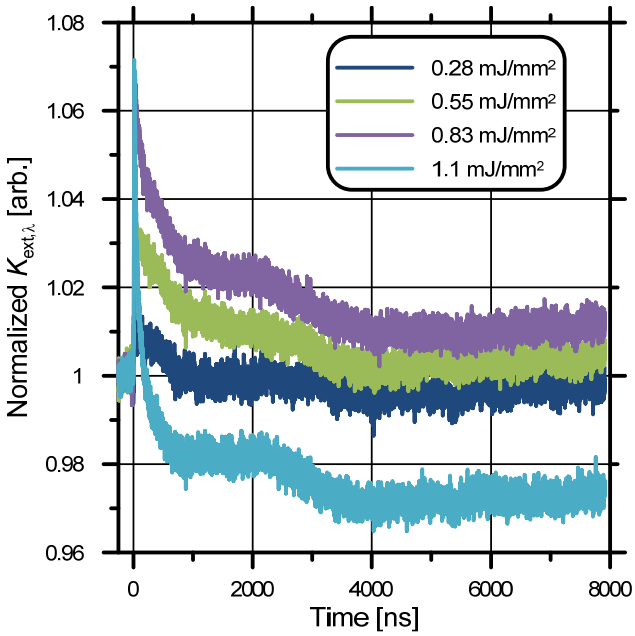

Figure 9 – normalized line-averaged 830 nm extinction coefficients for a range of pulse laser fluences

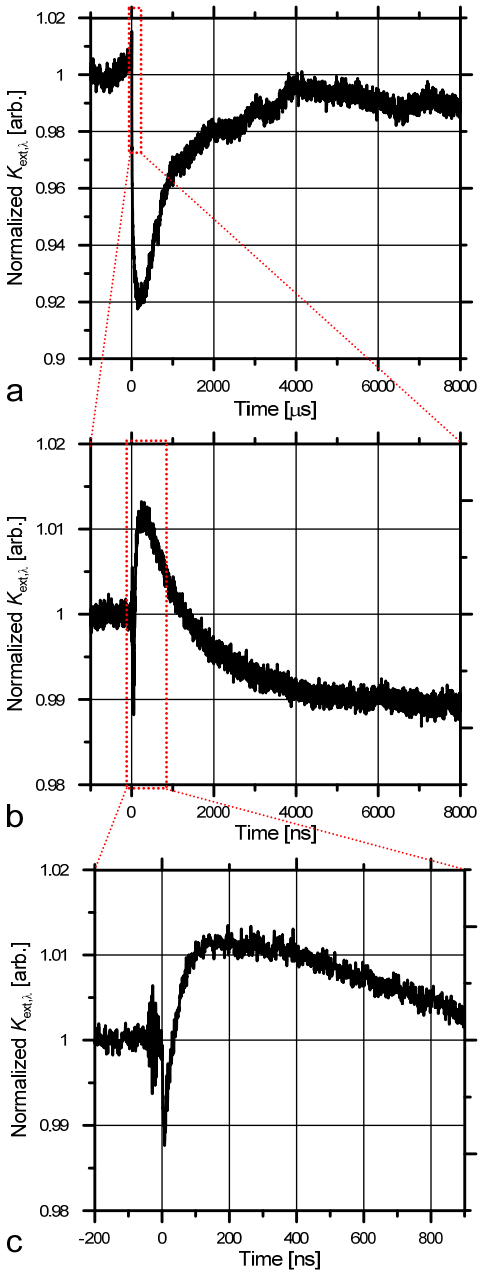

Figure 10 – normalized line-averaged 405 nm extinction coefficients for a laser fluence of 1.4 mJ/mm² for (a) long, (b) mid, and (c) short time intervals

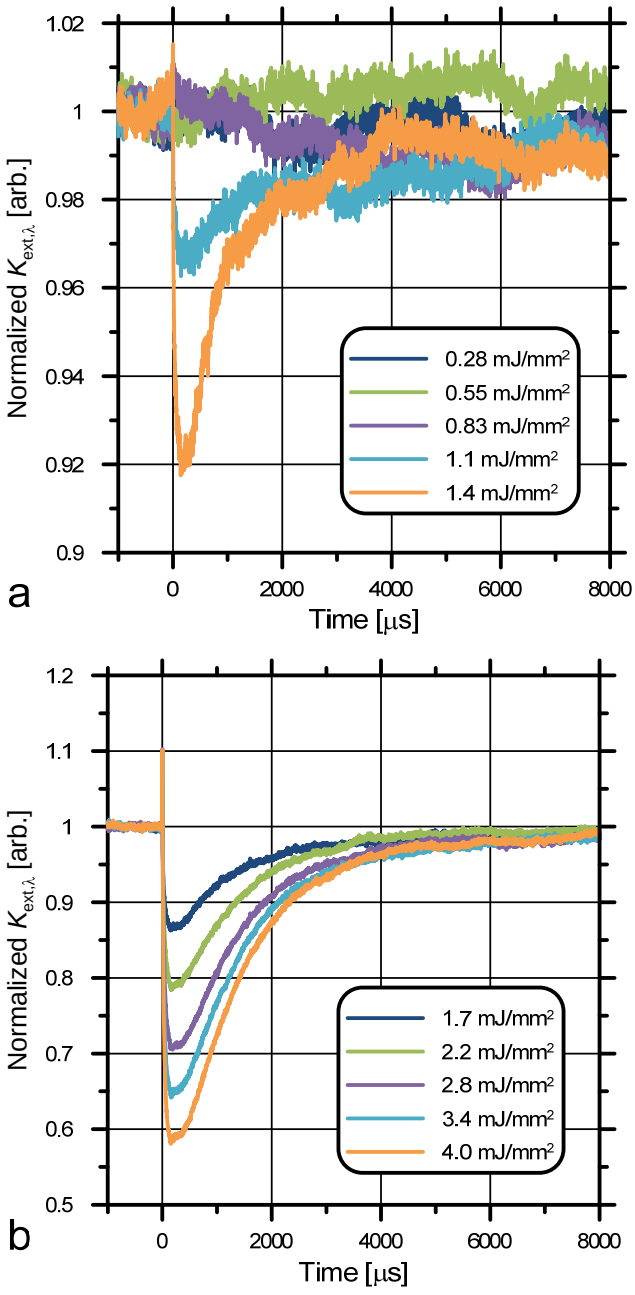

Figure 11 - normalized line-averaged 405 nm extinction coefficients for a range of pulse laser fluences (long time interval)

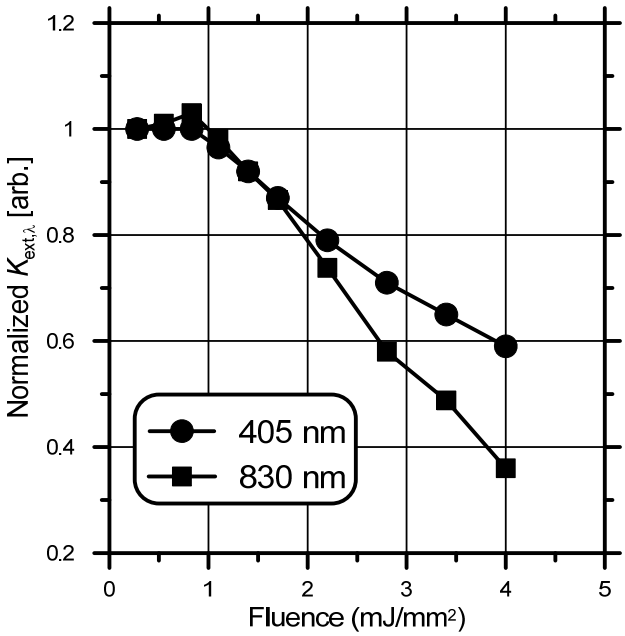

Figure 12 – minimum of normalized line-averaged 405 nm (300 µs after laser pulse) and 830 nm (1 µs after laser pulse) extinction coefficients for a range of pulse laser fluences

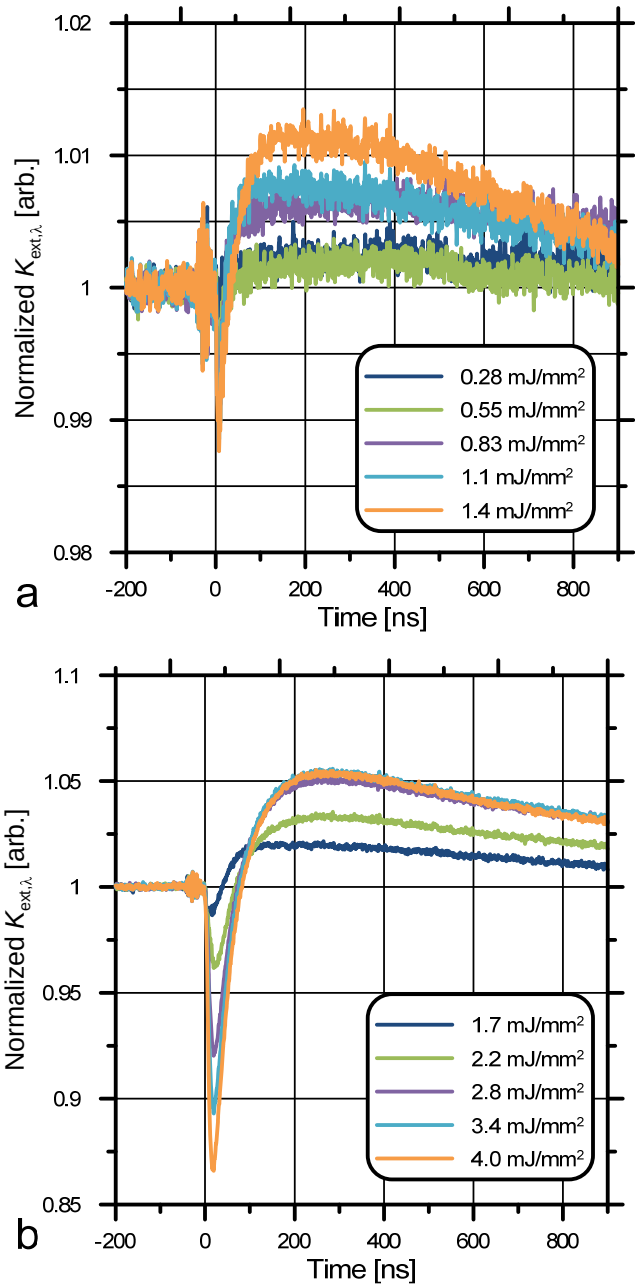

Figure 13 – normalized line-averaged 405 nm extinction coefficients for a range of pulse laser fluences (short time interval)

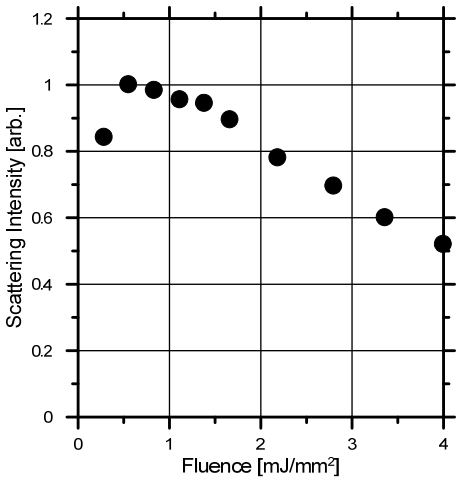

Figure 14 – normalized 1064 nm scattering intensity (measured scattering/fluence) versus fluence